Epoxy shape-memory polymer reinforced by thermally reduced graphite oxide: Influence of processing techniques

4 authors, including:

Wenbing Li
Harbin Institute of Technology
10 PUBLICATIONS   **113** CITATIONS

SEE PROFILE

Yanju Liu
Harbin Institute of Technology
107 PUBLICATIONS   **963** CITATIONS

SEE PROFILE

Leng Jinsong
Harbin Institute of Technology
381 PUBLICATIONS   **4,215** CITATIONS

SEE PROFILE

Some of the authors of this publication are also working on these related projects:

Project Shape memory polymers View project

Project Structural health monitoring View project

Epoxy shape-memory polymer reinforced by thermally reduced graphite oxide: Influence of processing techniques

Lei Chen,[1] Wenbing Li,[2] Yanju Liu,[1] Jinsong Leng[2]

[1]Department of Astronautical Science and Mechanics, Harbin Institute of Technology (HIT), Harbin, People's Republic of China
[2]Centre for Composite Materials, Science Park of Harbin Institute of Technology (HIT), Harbin, People's Republic of China
Correspondence to: Y. Liu (E-mail: yj_liu@hit.edu.cn) and J. Leng (E-mail: lengjs@hit.edu.cn)

ABSTRACT: In this article, epoxy shape-memory polymer (ESMP) reinforced with 1 wt % thermally reduced graphite oxide (TrGO) was fabricated by solution blending and three-roll mill (TRM) mixing, respectively. Both blending techniques allowed a uniform TrGO dispersion in ESMP matrix, and the TRM mixing lead to an exfoliation of the TrGO worms. Compared with pristine ESMP, the TrGO/ESMP composites showed 36.4–41.1% increase in Young's modulus and 38.1–44.1% improvement in tensile strength. The TrGO/ESMP composite fabricated by TRM mixing had a $T_{5\%}$ (the temperature where the material lost 5% of its initial weight) 16.4°C higher than pure ESMP. Compared with pure ESMP, a significant improvement of recovery force by 84.4% and 311.1% was obtained by TrGO/ESMP composite fabricated by solution blending and TRM mixing, respectively. © 2015 Wiley Periodicals, Inc. J. Appl. Polym. Sci. **2015**, *132*, 42502.

INTRODUCTION

Shape-memory polymers (SMPs) are a class of smart materials that can transform from one shape into another in response to external stimulus such as heat, light, electric or magnetic field.[1] A typical shape memory cycle often involves: (a) deformation of a SMP at above its shape memory transition temperature, (b) fixation of the deformed shape upon cooling under the deformation load, and (c) recovery of the original shape by reheating above the transition temperature.[2] SMPs include shape-memory polyurethane (SMPU), polystyrene-based SMP (PS-SMP), epoxy-based SMP (ESMP), and others.[1] In comparison with shape memory alloys and shape memory ceramics, SMPs have a number of intrinsic advantages including larger deformation strain, easier to manufacture, lower manufacturing cost, lower density, and many more varieties in actuation approaches.[3] These unique characteristics enable the SMPs to be used in a myriad of fields, including clothing manufacturing, automobile engineering, aerospace engineering, medical treatment, and many other applications.[4] However, pure SMPs are not suitable for some practical applications (for example, aerospace engineering) that require improved mechanical strength, higher thermal stability, and stronger shape recovery force. Therefore, SMPs filled with various reinforcement particles (such as SiC,[5] nanoclay,[6] carbon black,[7] carbon nanotubes,[8] graphene,[9] and hybrid fillers,[10,11]) were prepared and measured in order to

meet the requirements. Among these fillers, carbonaceous materials are superior to the others because of their high surface areas and excellent mechanical, thermal, and electrical properties.[7–11] The reported SMP composites filled by carbonaceous fillers focused on SMPU composites[7,9,11] and PS-SMP composites,[12,13] while carbon-filled ESMP has been barely studied.

As a newly developed carbonaceous material, thermally reduced graphite oxide (TrGO) is generally produced by heating graphite oxide (GO).[14] TrGO maintains the layered structure similar to graphite but produces tremendous different size of pores and nanosheets with high aspect ratios. One of the most potential applications of TrGO is its use as reinforcement filler in polymer composites.[15] TrGO can be easily filled by polymer monomers through physical adsorption because of its porous features and the interactions between the monomers and the polar groups on the TrGO layers.[14] After the TrGO was filled with monomers, in situ polymerization was usually carried out to form a TrGO/polymer composite. Polymers reinforced with TrGO show substantial improvements in mechanical property,[16] electrical conductivity,[17] and other properties over the unmodified polymers. However, to our best knowledge, ESMP reinforced with TrGO has not been fabricated, and the structure and property of the TrGO/ESMP composite have not been investigated so far. In this study, 1 wt % TrGO reinforced ESMP samples were fabricated and their structures, mechanical

properties, thermal stabilities, and shape recovery behaviors were studied. Moreover, the structures and properties of the TrGO/ESMP composites synthesized by different processing techniques were compared. These measurements indicate that TrGO can be used as very promising reinforcement filler for ESMP composites with improved mechanical property, higher thermal stability, and stronger recovery force, compared with unmodified ESMP.

EXPERIMENTAL

All chemical reagents used were of analytic purity or better. GO was synthesized by Hummer's method.[18] In a typical experiment, dried graphite powder (30 g, Sigma Aldrich, particle size: less than 20 μm) was put into a mixture of concentrated H_2SO_4 (500 mL) and $NaNO_3$ (10 g) kept in an ice bath (0°C). $KMnO_4$ (90 g) was added gradually under stirring so as to keep the temperature below 20°C. The mixture was stirred for 2 h and then the temperature of the mixture was increased to 35°C and kept for about 2 h, followed by dilution with distilled water. The mixture was stirred for 1 h again and then H_2O_2 (30%, 200 mL) was added gradually to the mixture. Upon the addition of the H_2O_2, the mixture turned bright yellow while bubbling. The mixture was stirred for another 1 h. Then the sediments were washed with 10% HCl solution, followed by repeated washing with distilled water until the pH of the solution became neutral. The final GO slurry was dried at 80°C and then pulverized with a ball mill to obtain fine GO powder.

TrGO was synthesized by reduction of GO with a rapid heating process. Firstly, a tube furnace was heated to 250°C under argon gas. Secondly, dried GO powder (1–3 g) was inserted quickly into the center of the furnace. Then the furnace was maintained at 250°C for about 5 min and subsequently cooled naturally to room temperature under argon. In this process, the GO was exfoliated due to the very fast evaporation of water, carbon dioxide and carbon monoxide.[14] The black powder of very low density deposited on the inner wall of the furnace was collected and denoted as TrGO.[15] Before the preparation of TrGO/ESMP composites, the TrGO was dried at 60°C for at least 4 h to minimize its water content.

ESMP resin in this study consists of epoxy resin, hardener, accelerator, and linear epoxy monomer.[19] The detailed chemical composition of the ESMP is proprietary to our laboratory, although the structure is known to be a thermoset crosslinked network. For the curing of the resin, the resin was cast into a flat glass mould and cured at 80°C for 1 h, followed by postcure at 150°C for 6 h in air.

Preparation of TrGO/ESMP composite by solution blending: the ESMP resin was first diluted with acetone before adding dried TrGO. Then the ESMP resin–acetone–TrGO mixture (mass ratio, TrGO : ESMP = 1 : 99) was stirred mechanically at room temperature for 30 min, followed by sonication at 150 W for 15 min. The mixture was stirred overnight at room temperature and then dried at 70°C under stirring for a few hours to ensure complete evaporation of the acetone. The mixture was cast into a flat glass mould and cured at 80°C for 1 h, followed by

postcure at 150°C for 6 h in air. The obtained composite sample is denoted as composite A.

Preparation of TrGO/ESMP composite by three-roll mill (TRM) mixing: the preparation of TrGO/ESMP composite by TRM mixing is similar to the process used by Yasmin *et al.*[20] A TRM (EXAKT 80E, EXAKT Advanced Technologies GmbH, Germany) was used in this study. Firstly, a mixture of uncured ESMP resin and dried TrGO (mass fraction of TrGO: 1%) was stirred with a glass bar. Then the mixture was poured between the feed and center rolls of the TRM and the rolls were allowed to start moving. Compounding was carried out at room temperature for about 4 h with a rotation speed of 300 rpm. The final product from the mill was collected and cast into a flat glass mould and cured at 80°C for 1 h, followed by postcure at 150°C for 6 h in air. The resultant composite sample is denoted as composite B.

The following measurements were used to characterize materials. Scanning electron microscope (SEM) analyses were performed with an environmental microscope (FEI-Quanta 200F). Before SEM analysis, the samples were vacuum coated with a thin gold layer using a precision etching coating system (Model 682, Gatan, USA) and the duration was 10 min. Fourier transform infrared (FTIR) spectra were recorded with a Nicolet 6700 FT-IR (Thermofisher Scientific, USA) using pellets in KBr. Nitrogen adsorption–desorption isotherms were collected on an ASAP 2420 (Micrometrics Instruments) nitrogen adsorption apparatus at 77 K. Prior to the measurements, the samples were pretreated by outgassing in a vacuum oven at 180°C for 10 h. For measuring the mechanical properties of the materials, they were cut into dumbbell specimens according to the ASTM D638 test method. The specimens were 3 mm thick with dimensions of 115 mm (L) × 19 mm (W) at the ends and 33 mm (L) × 6 mm (W) at the narrow part. The mechanical properties of the specimens at room temperature (20°C) were measured using a materials testing machine (Z050, Zwick/Roell) and the following measurement conditions were used: gauge length, 25 mm; crosshead speed, 5 mm/min; load cell, 50 kN; and preload, 8 N. A minimum of five specimens were tested for each material to obtain average values and standard deviations. Thermogravimetric analysis (TGA) was conducted from room temperature to 600°C under 50 mL/min air flow (TGA/DSC 1, Mettler Toledo) to measure their thermal stabilities. The heating rate was 10°C/min. Differential scanning calorimetry (DSC) experiments were carried out using DSC1 (Mettler Toledo) under nitrogen environment. The specimens were heated from 25°C to 175°C at a heating rate of 10°C/min. A dynamic mechanical analyzer (DMA/SDTA861, Mettler Toledo) in tension mode was used to measure the dynamic mechanical properties of the materials. Scanning measurements were performed between 25°C and 175°C from 1 Hz at a heating rate of 10°C/min.

Unconstrained shape recovery test included four steps.[12,21] First step, cured materials were cut into rectangular strips (length × width × thickness: 82 mm × 10 mm × 3 mm) and heated to 140°C. Second step, the strips were bent into a "U" shape circling a center axes, which had a diameter of 10 mm. The maximum bending angle was recorded as θ_{max}. Third step, the U-shaped specimens were cooled down at room temperature under the constant external force. This force was then removed
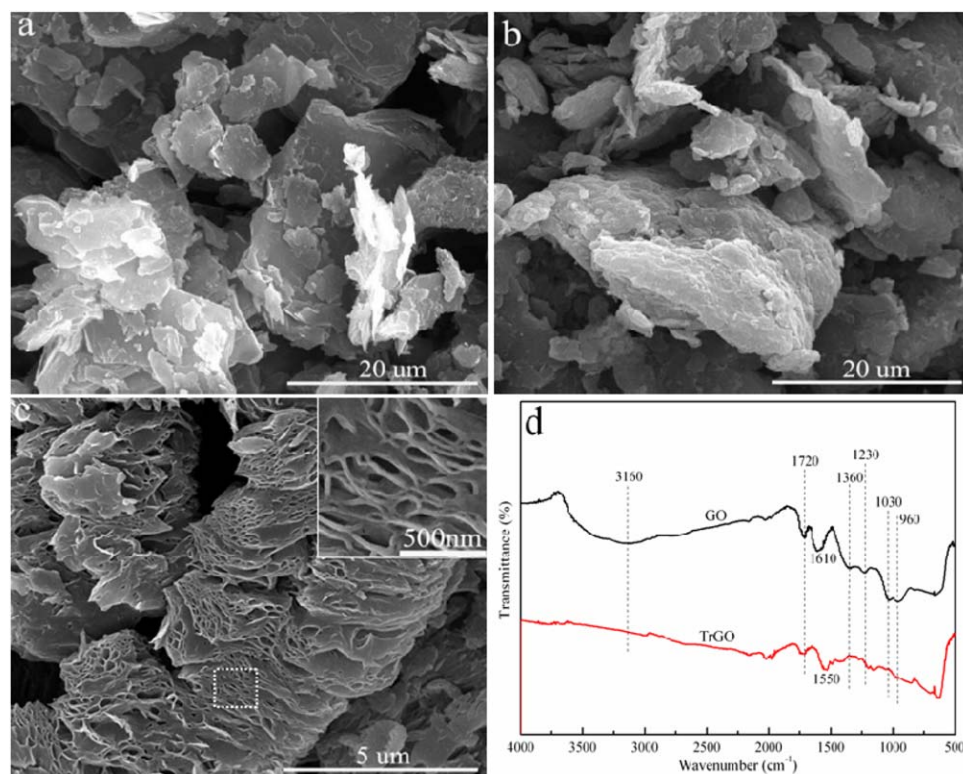
Figure 1. SEM images of graphite (a), GO (b), and TrGO (c), inset of image (c) is a magnification for the selected area; (d) FT-IR spectra of GO and TrGO. [Color figure can be viewed in the online issue, which is available at wileyonlinelibrary.com.]

after holding for several minutes. A marginal recovery occurred and the bending angle was reduced to θ_{fixed}. Last step, the bent specimens were put into a chamber preheated to 120°C. Then, the bending angle (θ_i) was recorded as a function of heating time. Three specimens were tested for each material to obtain average values and standard deviations for shape recovery times.

Shape retention ratio (R):[22]

$$R = \frac{\theta_{fixed}}{\theta_{max}} \times 100\% \qquad (1)$$

In the process for unconstrained shape recovery test, for both pure ESMP and the TrGO/ESMP composites, the differences between θ_{max} and θ_{fixed} were always less than 2°, so all of these specimens have an R of more than 99%.

Shape recovery ratio (R_r):[22]

$$R_r = \frac{\theta_{max} - \theta_i}{\theta_{max}} \times 100\% \qquad (2)$$

The process for recovery force test included four steps.[5] First, cured ESMP was cut into rectangular strips with the same length (55 mm) and thickness (3 mm) but different widths (6, 8, 10, and 12 mm, respectively); composite A and composite B were cut into rectangular strips (length: 55 mm, thickness: 3 mm, and width: 12 mm). Second, the strips were heated to 140°C and kept for 5–10 min. Third, the strips were bent into curves with an inner diameter of 35 mm, and then cooled to room temperature under constraint. Fourth, the curved specimen was placed in the three-point bend fixture of a DMA instrument (DMA1, Mettler Toledo), the probe tip was brought

just into contact with the inner surface of the specimen, and then the temperature was increased with a heating rate of 4°C/min while the probe tip was kept by displacement control. Upon increasing the temperature, the bent specimen released a force (i.e., the recovery force) compressing the probe tip because the bent specimen "wanted" to return to its original rectangular shape as a result of shape memory effect.

RESULTS AND DISCUSSION

Structure Characterizations of TrGO

In order to characterize the structural changes from graphite to GO and to TrGO, SEM characterizations were carried out and the results are shown in Figure 1(a–c). The graphite flakes show a sharp and keen-edged boundary, while the boundaries of GO have been broken because of oxidation. As shown in Figure 1(c), the TrGO are worm like and rough in surface. The inset image in Figure 1(c) indicates the TrGO worms are loosely bonded and porous, and the exfoliated graphite nanosheets in the TrGO have a thickness of 30–40 nm. FTIR was employed to analyze the existence of functional groups in GO and their changes after the thermal shock, as shown in Figure 1(d). For GO, the peaks at 1720, 1360, 1230, 1030, and 960 cm^{-1} signify the presence of carboxyl, epoxy, and hydroxyl functional groups.[23] As a consequence, the GO is hydrophilic, which is evidenced by the broad water peak at 3160 cm^{-1} and the second water peak at 1610 cm^{-1}.[24] After the thermal shock, the peaks from oxygen-containing groups decrease in intensity for TrGO as a result of decomposition. And a peak at 1550 cm^{-1} appears for TrGO, which corresponds to the C═C vibrations from un-
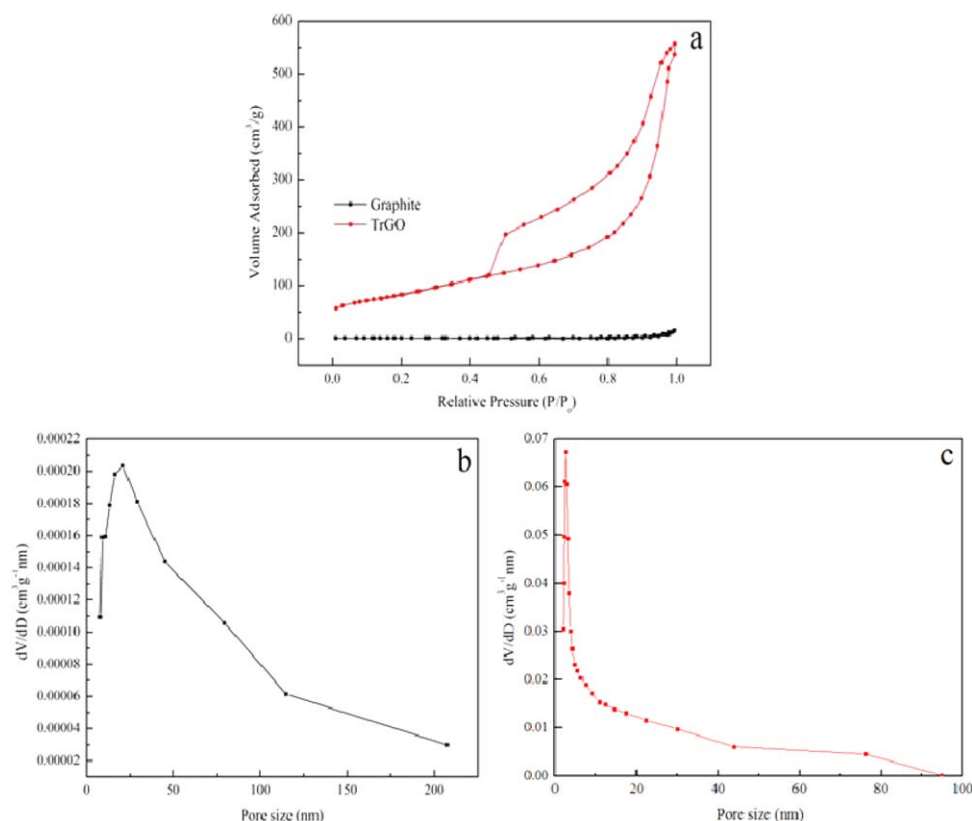
Figure 2. N_2 adsorption–desorption isotherms of graphite and TrGO (a); BJH (Barrett–Joyner–Halenda) pore size distributions from adsorption branches for graphite (b); and TrGO (c). [Color figure can be viewed in the online issue, which is available at wileyonlinelibrary.com.]

oxidized graphitic domains. Therefore, the TrGO becomes hydrophobic, which is evidenced by the disappearance of the absorption peaks corresponding to water (3160 cm^{-1} and 1610 cm^{-1}). These evidences indicate that the GO has been reduced by the thermal shock. It is important to note that the TrGO still contains some residual oxygen-containing groups such as C=O (the peak at 1720 cm^{-1}), which are assumed to promote both physical and mechanical interactions between the TrGO and polymers.[25]

The pore characteristics of graphite and TrGO were quantitatively analyzed using cryogenic (77 K) nitrogen adsorption–desorption isotherms, as shown in Figure 2 and Table I. The adsorption–desorption isotherms of graphite indicate that it is nonporous, based on the observation of a Type-II-like adsorption isotherm, in accordance with the classification guidelines provided by the International Union of Pure and Applied Chemistry.[26] In contrast, TrGO exhibits typical Type-IV characteristics, i.e., a steep increase at intermediate pressures with hysteresis. These properties indicate the development of porosity in the TrGO, possibly due to the formation of crumpled and folded graphite nanosheets, as confirmed by the SEM image in Figure 1(c). Huge increases in the Brunauer–Emmett–Teller (BET) surface area and pore volume of the TrGO of up to 296 m^2/g (>100 times than that of raw graphite) and 0.845 cm^3/g (>35 times than that of raw graphite) are observed, as shown in Table I. In terms of pore size distribution [see Figure 2(c)], the TrGO shows a large proportion of mesopores and

a few macropores. These results demonstrate that highly porous TrGO can be prepared by a rapid heating process, even under low-temperature reduction conditions (250°C).

Structures and Properties of Pure ESMP and TrGO/ESMP Composites

In order to investigate the dispersion states of the TrGO in the composites, fracture surfaces of the composite A and the composite B were characterized by SEM, as shown in Figure 3. In both composites, isolated TrGO particles are dispersed homogeneously in the polymer matrix, which indicates both processing techniques are efficient for uniformly dispersing TrGO into the ESMP. In addition, two different TrGO structures are observed within the polymer by varying the processing techniques. In the composite A, the TrGO particles maintain their original, expanded shape, as shown in Figure 3(a, b). In Figure 3(a), less than five TrGO worms can be observed. However, because of the shear force of the TRM, the TrGO in the composite B are exfoliated into many small particles, as shown in Figure 3(c). In Figure 3(c), more than 15 TrGO particles can be found. The average size of these particles is about 5 μm, as indicated by Figure 3(d). In both composites, the exposed graphite nanosheets can be seen clearly, as indicated by the arrows in Figure 3(b, d). The pores among these graphite nanosheets have been fully filled by the polymer matrix, and a good interfacial adhesion between the TrGO and the polymer matrix can be seen. The fracture surface SEM image of pure ESMP is also shown for comparison [Figure 3(e, f)]. Unlike the rough fracture

Table I. BET Surface Areas, Pore Volumes, and Average Pore Sizes of Graphite and TrGO

Sample	BET surface area (m^2 g^{-1})	Pore volume (cm^3 g^{-1})	Average pore size (nm)
Graphite	2.3	0.022	44.5
TrGO	296	0.845	10.7

surface of the TrGO/ESMP composites, the fracture surface of pure ESMP is very smooth.[22]

Figure 4(a) shows the photo of the dumbbell specimens of pure ESMP, composite A and composite B. It is shown that pure

ESMP dumbbell is transparent, while the composite dumbbells are nontransparent. This is due to the uniform dispersion of TrGO in the ESMP in both composites, which leads to a strong reduction in transmission. Figure 4(b) shows typical stress–strain curves of these dumbbells measured at room temperature, and the results are summarized in Table II. The Young's modulus and tensile strength of pure ESMP at room temperature are ~1.29 GPa and ~41.31 MPa, respectively. Compared with pure ESMP, the composite A provides 36.4% increase in Young's modulus and 38.1% increase in tensile strength, whereas the composite B exhibits 41.1% increase in Young's modulus and 44.1% increase in tensile strength. The improvements in Young's modulus and tensile strength of the ESMP upon the addition of TrGO are attributed to the uniform dispersion of the TrGO in
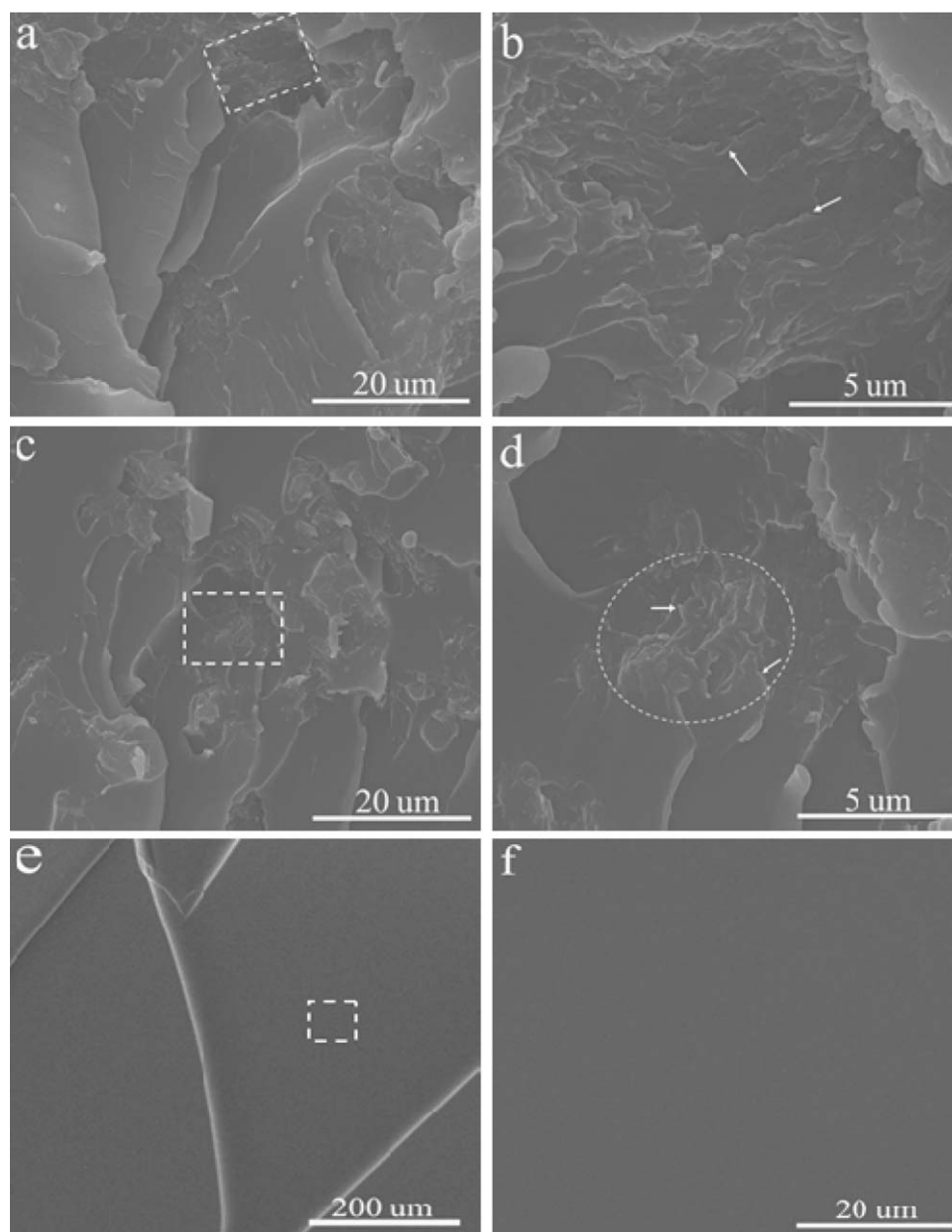

Figure 3. Fracture surface SEM images of composite A (a and b), composite B (c and d), and pure ESMP (e and f). Images (b), (d), and (f) are the magnified images for the selected areas in (a), (c), and (e), respectively.
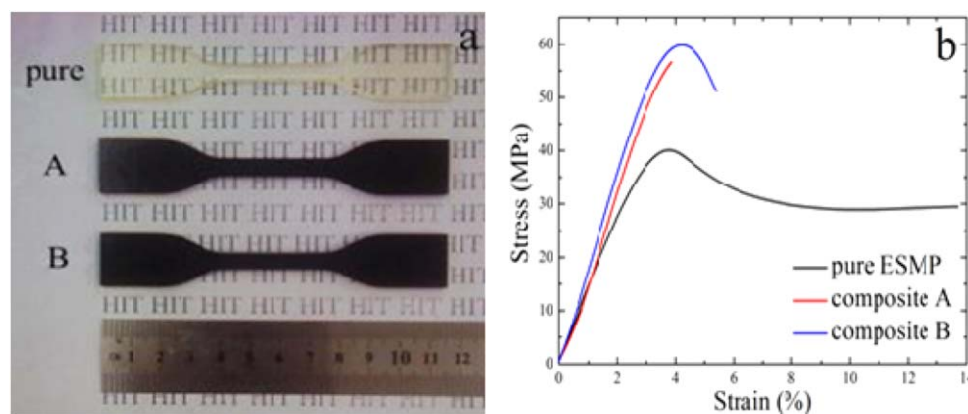
Figure 4. (a) Photo of dumbbell specimens and (b) typical tensile stress–strain curves measured at room temperature of pure ESMP, composite A, and composite B. [Color figure can be viewed in the online issue, which is available at wileyonlinelibrary.com.]

the ESMP and the good interfacial adhesion between the TrGO and the polymer matrix (as shown in Figure 3), so that the mobility of the polymer chains is restricted under loading.[27] As shown in Figure 3(a, c), TrGO are homogeneously distributed in both composite A and composite B, and no aggregations are observed. Moreover, the TrGO contains considerable number of C=O groups [evidenced by FTIR spectra in Figure 1(d)] on its surface, which enhance the interaction between TrGO and epoxy-based matrix. Therefore, the polymer chains can easily be intercalated into the gallery of TrGO and as a result, no delaminations are found in the interfaces between TrGO and polymer matrix, as shown in Figure 3(b, d). The composite B has higher Young's modulus and higher tensile strength than the composite A. This result can be attributed to two reasons. Firstly, the big TrGO particles in the composite A may have some cracks in their inner part where there is virtually no bond with the polymer matrix,[28] and these defects can initiate easily the fracture of the composite A. However, for the composite B, the external shear force generated by the TRM has exfoliated the TrGO into smaller particles, as shown in Figure 3(c, d). As a consequence, polymer chains enter the pores of the small TrGO particles easily and fill most of the cracks, thus forming a stronger adhesion between the TrGO and the polymer than the composite A. Secondly, as a result of exfoliation, the small TrGO particles in the composite B have a higher surface area than the big TrGO particles in the composite A. It has been reported that a higher surface area of fillers can provide a better interaction between the fillers and polymer matrix.[29] So the composite B shows improved Young's modulus and higher tensile strength than the composite A. It is also noted that the fracture elongations of

both TrGO/ESMP composites are reduced compared with pure ESMP and especially larger reduction is observed for the composite A. The lower fracture elongation of the composite A, compared with the composite B, may be because the inner cracks of the TrGO in the former can initiate the fracture of the composite easily.

In order to better understand the effect of TrGO and its dispersion state on the thermal stability of ESMP matrix, the thermal degradation behaviors of pure ESMP and its TrGO composites were examined via TGA, as shown in Figure 5. As shown in Figure 5(a), pure ESMP and its composites begin to lose weight at about 200°C and decompose in a two-step process, attributable to the soft and hard segments in ESMP, respectively. It is obvious that the initial weight loss of the composites by thermal degradation is retarded by the presence of TrGO, as shown in Figure 5(b). This may be due to the heat shielding effect of TrGO in the polymer composites[30] and formation of mass transport barrier to the volatile products produced during the decomposition of the composites.[31] In polymer/graphite composite, the thermal stability was generally enhanced by the graphite because it hindered the diffusion of volatile decomposition products. For example, Rajkumar *et al.* found a higher thermal stability for nanographite loaded nitrile butadiene rubber composites with increasing in nanographite loadings;[32] Quan *et al.* observed a positive effect of graphite nanoplatelets (GNPs) on the thermal stability of the GNPs-filled thermoplastic polyurethane nanocomposites.[33] The temperature at which the material loses 5% of its initial weight is defined as $T_{5\%}$.[30] As shown in Figure 5(b), pure ESMP has a $T_{5\%}$ of 328.1°C, while the composite A and the composite B have $T_{5\%}$ of 332.1°C and 344.5°C, respectively. This means that the composite B has a higher $T_{5\%}$ than the composite A. This indicates that the barrier effect is more obvious for the composite B than the composite A. This may be because the small TrGO particles in the composite B (see Figure 3) have a better thermal shielding effect on the polymer matrix than the big TrGO particles in the composite A, as a result of higher surface area.

The glass transition is the essential transition from freezing to free motion states of segments in a polymer network, which is revealed by glass transition temperature (T_g). In this study, T_g

Table II. Tensile Stress-Strain Properties of Pure ESMP, Composite A, and Composite B Measured at Room Temperature (20°C)

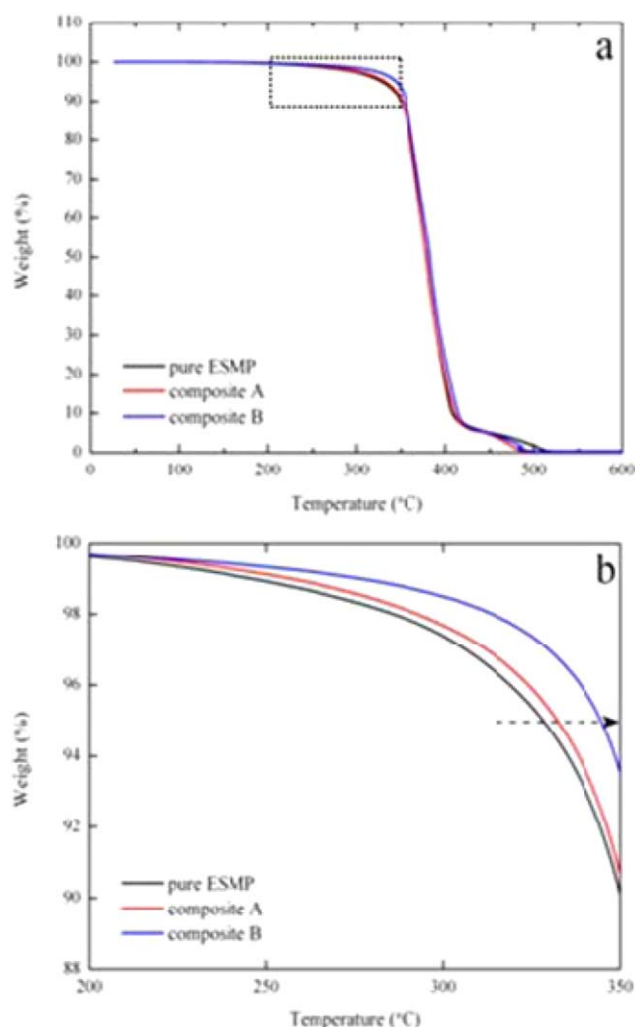| Materials	Young's modulus (GPa)	Tensile strength (MPa)	Fracture elongation (%)
Pure ESMP	1.29 ± 0.04	41.31 ± 1.22	13.71 ± 1.80
Composite A	1.76 ± 0.03	57.03 ± 1.14	3.86 ± 0.50
Composite B	1.82 ± 0.02	59.53 ± 1.06	5.40 ± 0.27

Figure 5. TGA curves of pure ESMP, composite A, and composite B measured in air flow (image b is a magnification for the selected area in image a). [Color figure can be viewed in the online issue, which is available at wileyonlinelibrary.com.]

of pure ESMP and the TrGO/ESMP composites are characterized using DSC and DMA, respectively, as shown in Figure 6. As shown in Figure 6(a), pure ESMP has a DSC T_g at 90.6°C (the inflection point), while the composite A and the composite B have a DSC T_g at 93.4°C and 97.3°C, respectively. These results indicate that the addition of TrGO increases the DSC T_g of the ESMP, and the composite B has a higher DSC T_g than the composite A. The DMA T_g of pure ESMP is found to be 98.2°C (peak value of tan δ[34]), as shown in Figure 6(b). Adding TrGO to the ESMP can increase its DMA T_g, which shows a similar trend to their DSC T_g. This observation is attributed to the restricted segmental movement upon the addition of fillers.[35] Different processing techniques lead to different DMA T_g of the composites: the composite B has a higher DMA T_g (108.1°C) than the composite A (103.7°C), which also shows a similar trend to the DSC T_g. This may be because the uniformly dispersed small TrGO particles in the composite B have a more efficient restricting effect on the polymer chains than the big TrGO worms in the composite A. The DMA T_g values are

7–11°C higher than the DSC T_g, due to the frequency effect in DMA test.[36] According to the curves of storage modulus E' [see Figure 6(b)], the E' at room temperature increases from about 1.3 GPa of pure ESMP to approximately 1.8 GPa of the TrGO/ESMP composites. The E' of the composite B is higher than that of the composite A. This also indicates the better reinforcing effect of TrGO when embedded into the ESMP through TRM mixing than solution blending.

Shape Recovery Behaviors of Pure ESMP and TrGO/ESMP Composites

One of the most critical properties of SMPs and their composites are shape recovery behaviors. For example, Figure 7(a) shows the unconstrained shape recovery of a U-shaped composite B specimen at 120°C. A decrease of the bending angle (θ_i) is observed with increased heating time, and the specimen recovers from temporary U shape to original rectangular shape in 10 min. The relationship between shape recovery ratio (R_r) and heating time for different materials are shown in Figure 7(b), and their shape recovery times are compared in Figure 7(c). The shape recovery times of the composites are longer than that of pure ESMP (170 ± 10 s), and the composite B has a longer shape recovery time (570 ± 15 s) than the composite A
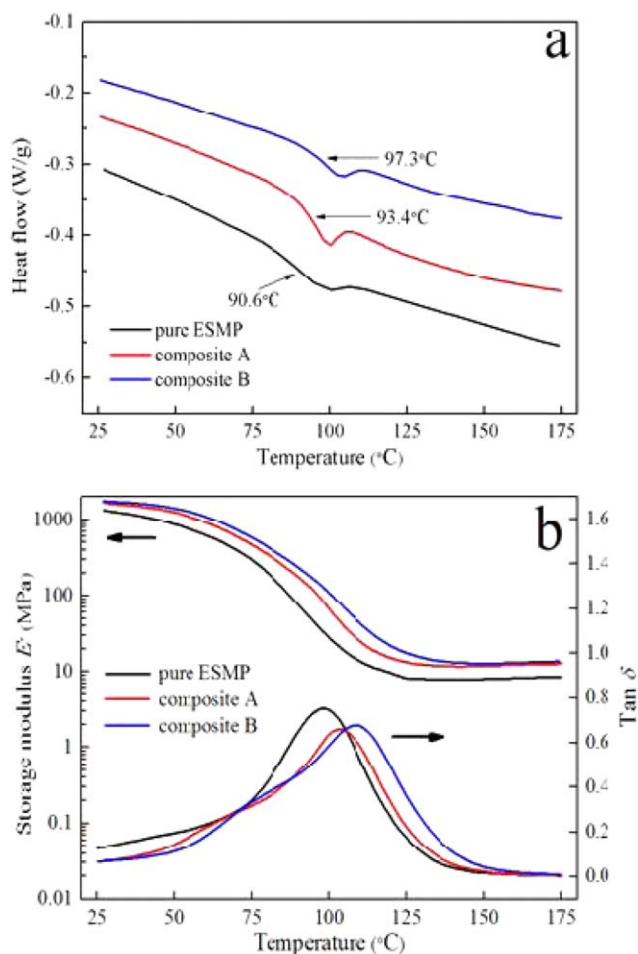

Figure 6. (a) DSC curves, (b) storage modulus E' and tan δ curves of pure ESMP, composite A, and composite B. [Color figure can be viewed in the online issue, which is available at wileyonlinelibrary.com.]
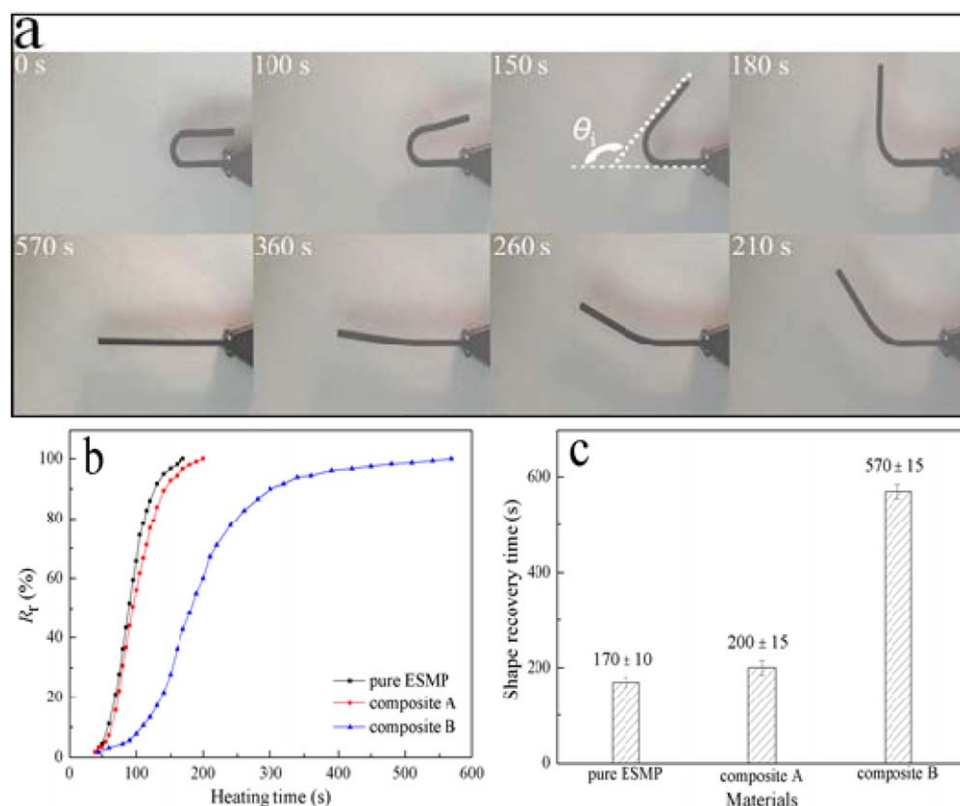
Figure 7. (a) Shape recovery process of composite B specimen, (b) typical relationship between shape recovery ratio (R_r) and heating time, and (c) shape recovery times of different materials at 120°. [Color figure can be viewed in the online issue, which is available at wileyonlinelibrary.com.]

(200 ± 15 s). The longer shape recovery time of the composites compared with pure ESMP may be because the TrGO particles restrict the polymer chains from freedom moving as a result of the uniform dispersion of TrGO in ESMP and the good interfacial interactions between them, as shown in Figure 3. And therefore, compared with pure ESMP, the polymer chains in the composites need a longer duration to reach their original positions when heated above the material's T_g temperature. A longer shape recovery time of composite B than composite A can be attributed to the stronger restriction effect on the polymer chains by the exfoliated, small TrGO particles in the composite B than the intact, big TrGO particles in the composite A. A stronger restriction on the movement of the polymer chains leads to a harder and slower movement of the chains to their initial states upon heating above T_g. As a result, a stronger restriction leads to a longer shape recovery time of the bent specimen.

Recovery Forces of Pure ESMP and TrGO/ESMP Composites

Besides shape recovery time, recovery force is also very important for SMPs and their composites.[5,37] The setup used to test recovery force by a DMA instrument under fixed displacement is illustrated by the inset in Figure 8(a). The influence of width on the recovery forces of pure ESMP specimens is investigated here, as shown in Figure 8(a). The change of the recovery force as a function of temperature can be divided into three steps. First step, as the temperature increases from 25°C to about 45°C, the recovery force increases slowly and almost linearly.

Second step, a sharp increase of the recovery force is observed by increasing the temperature above 45°C, and a peak value of the recovery force is reached at around 60°C (55–65°C), as indicated by arrows in Figure 8(a). Third step, after the recovery force reaches its peak value, it decays gradually with further increase of the temperature and finally reaches a steady state. As the soft segment crystals melt with increasing temperature, the bent specimen attempts to straighten and applies a compressive force on the probe tip of DMA setup. In order to keep the deformed shape constant, the DMA applies the same amount of force to balance the straightening force. This force is referred as the recovery force. When a certain high temperature is reached, the molecular chains become softer once all soft segment crystals are melted, and the specimen begins stress relaxation.[6,38] The peak value of the recovery force is defined as F_{max}. It is obvious that pure ESMP specimen with larger width exerts a higher F_{max}, and the ESMP specimen with a width of 12 mm releases aN F_{max} of 450 mN at 65°C. Figure 8(b) compares the constrained bend recovery forces of pure ESMP, composite A, and composite B specimens with the same width of 12 mm. The recovery force curves of the composite specimens have a similar trend to that of pure ESMP. The composite A specimen has an F_{max} of 830 mN at 80°C and the composite B specimen releases a F_{max} of 1850 mN at 94°C, as indicated by the arrows in Figure 8(b). Compared with the F_{max} of pure ESMP specimen, the composite A specimen shows an improvement of 84.4%, while the composite B specimen shows an improvement of 311.1%. It has been reported that adding 20 wt % SiC
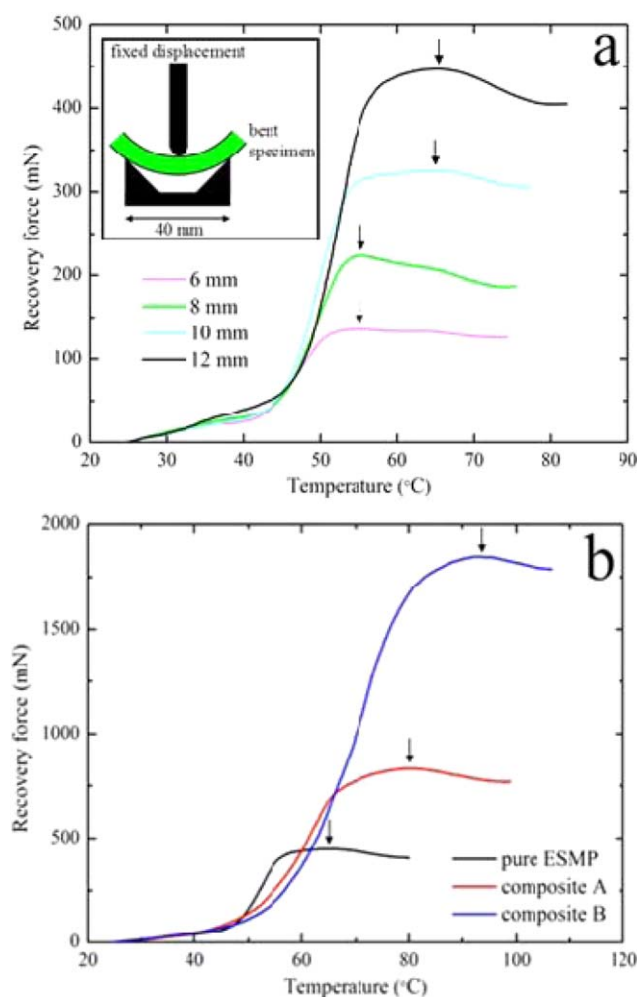
Figure 8. (a) Constrained bend recovery force as a function of temperature for pure ESMP specimens with different widths, the inset shows the setup used to test the constrained bend recovery force in the DMA instrument; (b) constrained bend recovery force as a function of temperature for pure ESMP, composite A, and composite B specimens with the same width of 12 mm. [Color figure can be viewed in the online issue, which is available at wileyonlinelibrary.com.]

nanoparticles into ESMP only provided a 50% improvement to its F_{max}.[5] Compared with SiC, the TrGO can improve the recovery force of ESMP more obviously with a much lower filler content (1 wt %). This is mainly due to its high surface area and good interfacial adhesions with the ESMP matrix.[9] The F_{max} value of a SMP or its composite is mainly determined by the material's mechanical properties.[6,38] As discussed before, the TrGO has a large specific surface area and a few oxygen-containing groups on its surface. As a result, the TrGO in the ESMP composites has a relatively strong restriction on the polymer chains, and the mechanical properties of the TrGO/ESMP composites are enhanced compared with pure ESMP, as evidenced by tensile tests and DMA measurements. Therefore, the F_{max} of the TrGO/ESMP composites are higher than pure ESMP. The higher recovery force of the composite B specimen compared with the composite A specimen may be because the TrGO particles in the composite B are smaller and have a higher

surface area than the big TrGO particles in the composite A. The obvious exfoliation of TrGO worms in the composite B (see Figure 3) enables them a stronger restriction on the polymer chains than the big TrGO worms in the composite A. As a result, the composite B shows improved mechanical properties than the composite A, as proved by tensile tests and DMA measurements. So the F_{max} of the composite B is higher than the composite A, as shown in Figure 8(b).

CONCLUSIONS

In this article, ESMP, a kind of smart polymer, reinforced by TrGO, a kind of porous, low cost, and scalable carbonaceous material synthesized by low-temperature reduction of GO, was fabricated. Two techniques were used for fabricating TrGO/ESMP composites. The effects of TrGO on the structure and properties of ESMP were examined. The conclusions can be summarized as follows:

1. Both techniques provided a uniform TrGO dispersion in the ESMP. The solution blending maintained the original structure of TrGO in the composite A, while the TRM mixing showed an obvious exfoliation of TrGO in the composite B.
2. The composite B had higher Young's modulus, thermal stability, and T_g than the composite A, which reflected a better reinforcement of the small TrGO particles in the composite B, compared with the big TrGO worms in the composite A.
3. Unconstrained shape recovery tests showed that adding 1 wt % TrGO increased the shape recovery time of ESMP. Constrained bend recovery force tests indicated that adding 1 wt % TrGO improved significantly the recovery force of ESMP, and the composite B provided a higher recovery force than the composite A.

ACKNOWLEDGMENTS

REFERENCES

1. Leng, J. S.; Lan, X.; Liu, Y. J.; Du, S. Y. *Prog. Mater. Sci.* **2011**, *56*, 1077.

2. Xiao, X. C.; Xie, T.; Cheng, Y. T. *J. Mater. Chem.* **2010**, *20*, 3508.

3. Lendlein, A.; Jiang, H. Y.; Jünger, O.; Langer, R. *Nature* **2005**, *434*, 879.

4. Meng, Q. H.; Hu, J. L. *Compos. Part A-Appl. S.* **2009**, *40*, 1661.

5. Gall, K.; Dunn, M. L.; Liu, Y. P.; Finch, D.; Lake, M.; Munshi, N. A. *Acta Mater.* **2002**, *50*, 5115.

6. Cao, F. N.; Jana, S. C. *Polymer* **2007**, *48*, 3790.

7. Gunes, I. S.; Cao, F. N.; Jana, S. C. *Polymer* **2008**, *49*, 2223.

8. Ni, Q. Q.; Zhang, C. S.; Fu, Y. Q.; Dai, G. Z.; Kimura, T. *Compos. Struct.* **2007**, *81*, 176.

9. Jung, Y. C.; Kim, J. H.; Hayashi, T.; Kim, Y. A.; Endo, M.; Terrones, M; Dresselhaus, M. S. *Macromol. Rapid Commun.* **2012**, *33*, 628.

10. Lu, H. B.; Lei, M.; Leng, J. S. *J. Appl. Polym. Sci.* **2014**, *131*, 40506.

11. Yi, D. H.; Yoo, H. J.; Mahapatra, S. S.; Kim, Y. A.; Cho, J. W. *J. Colloid Interface Sci.* **2014**, *432*, 128.

12. Lan, X.; Liu, Y. J.; Lv, H. B.; Wang, X. H.; Leng, J. S.; Du, S. Y. *Smart Mater. Struct.* **2009**, *18*, 024002.

13. Lu, H. B.; Liu, Y. J.; Gou, J. H.; Leng, J. S.; Du, S. Y. *Compos. Sci. Technol.* **2011**, *71*, 1427.

14. Yang, S. J.; Kim, T.; Jung, H.; Park, C. R. *Carbon* **2013**, *53*, 73.

15. Steurer, P.; Wissert, R.; Thomann, R.; Mülhaupt, R. *Macromol. Rapid Commun.* **2009**, *30*, 316.

16. Das, B.; Prasad, K. E.; Ramamurty, U.; Rao, C. N. R. *Nanotechnology* **2009**, *20*, 125705.

17. Kim, H.; Miura, Y.; Macosko, C. W. *Chem. Mater.* **2010**, *22*, 3441.

18. Hummers, Jr., W. S.; Offeman, R. E. *J. Am. Chem. Soc.* **1958**, *80*, 1339.

19. Leng, J. S.; Wu, X. L.; Liu, Y. *J. Smart Mater. Struct.* **2009**, *18*, 095031.

20. Yasmin, A.; Luo, J. J.; Daniel, I. M. *Compos. Sci. Technol.* **2006**, *66*, 1179.

21. Du, F. P.; Ye, E. Z.; Yang, W.; Shen, T. H.; Tang, C. Y.; Xie, X. L.; Zhou, X. P.; Law, W. C. *Compos. Part B-Eng.* **2015**, *68*, 170.

22. Zhao, L. M.; Feng, X.; Li, Y. F.; Mi, X. J. *Polym. Sci. Ser. A* **2014**, *56*, 640.

23. Dimiev, A.; Kosynkin, D. V.; Alemany, L. B.; Chaguine, P.; Tour, J. M. *J. Am. Chem. Soc.* **2012**, *134*, 2815.

24. Jeong, H. K.; Lee, Y. P.; Jin, M. H.; Kim, E. S.; Bae, J. J.; Lee, Y. H. *Chem. Phys. Lett.* **2009**, *470*, 255.

25. Song, L. N.; Xiao, M.; Meng, Y. Z. *Compos. Sci. Technol.* **2006**, *66*, 2156.

26. Sing, K. S. W.; Everett, D. H.; Haul, R. A. W.; Moscou, L.; Pierotti, R. A.; Rouquérol, J.; Siemieniewska, T. *Pure Appl. Chem.* **1985**, *57*, 603.

27. Wei, C. L.; Zhang, M. Q.; Rang, M. Z.; Friedrich, K. *Compos. Sci. Technol.* **2002**, *62*, 1327.

28. Li, J.; Kim, J. K.; Sham, M. L. *Scripta Mater.* **2005**, *53*, 235.

29. Cho, D.; Lee, S.; Yang, G.; Fukushima, H.; Drzal, L. T. *Macromol. Mater. Eng.* **2005**, *290*, 179.

30. Raghu, A. V.; Lee, Y. R.; Jeong, H. M.; Shin, C. M. *Macromol. Chem. Phys.* **2008**, *209*, 2487.

31. Malas, A.; Das, C. K.; Das, A.; Heinrich, G. *Mater. Design* **2012**, *39*, 410.

32. Rajkumar, K.; Kumari, N.; Ranjith, P.; Chakraborty, S. K.; Thavamani, P. *Int. J. Chem. Tech. Res.* **2011**, *3*, 1343.

33. Quan, H.; Zhang, B.; Zhao, Q.; Yuen, R. K. K.; Li, R. K. Y. *Compos: Part A* **2009**, *40*, 1506.

34. Castro, F.; Westbrook, K. K.; Hermiller, J.; Ahn, D. U.; Ding, Y. F.; Qi, H. J. *J. Eng. Mater.-T. ASME* **2011**, *133*, 021025.

35. Zheng, W. G.; Wong, S. C. *Compos. Sci. Technol.* **2003**, *63*, 225.

36. Merline Dyana, J.; Reghunadhan Nair, C. P.; Gouri, C.; Sadhana, R.; Ninan, K. N. *Eur. Polym. J.* **2007**, *43*, 3629.

37. Ahmad, M.; Singh, D.; Fu, Y. Q.; Miraftab, M.; Luo, J. K. *Polym. Degrad. Stab.* **2011**, *96*, 1470.

38. Yan, B. B.; Gu, S. Y.; Zhang, Y. H. *Eur. Polym. J.* **2013**, *49*, 366.